Editors' Suggestion

Small transition-metal dichalcogenide nanostructures down to subnanometer by two-dimensional material origami

Wen Zhao,[1,2] Xibiao Ren,[3] Bo Wang,[3] Chuanhong Jin,[3] Wenhui Duan,[2,*] and Feng Ding[1,4,†]

[1]*Center for Multidimensional Carbon Materials (CMCM), Institute for Basic Science (IBS), Ulsan 689-798, Republic of Korea*

[2]*Department of Physics and State Key Laboratory of Low-Dimensional Quantum Physics, Tsinghua University, Beijing 100084, China*

[3]*State Key Laboratory of Silicon Materials, School of Materials Science and Engineering, Zhejiang University, Hangzhou, 310027, China*

[4]*School of Materials Science and Engineering, Ulsan National Institute of Science and Technology (UNIST), Ulsan 689-798, Republic of Korea*

(Received 28 February 2019; published 24 May 2019)

Origami is a promising method for creating various structures from filmlike materials via local deconstruction rather than elastic bending. Transition-metal dichalcogenides (TMDCs) have high bending stiffness making the formation of highly curved nanostructures, such as nanotube or nanocages, via bending difficult. Here, we propose the use of two-dimensional (2D) material origami to build stable TMDC nanostructures. Various nanostructures, such as polygonal nanotubes or polyhedral nanocages, can be created by introducing line defects, which incurs only a very small energy penalty. Through first-principles calculations and high-resolution transmission electron microscopy imaging, we confirmed their stability and the possibility of synthesis experimentally via line defect formation. As an example, the widely observed TMDC nanowires are produced with this approach, and many experimentally observed nanostructures agree with these origami creases/line defects. This work opens a door to synthesize nanostructures of few-atomic-thick 2D materials for various potential applications.

DOI: 10.1103/PhysRevMaterials.3.056001

I. INTRODUCTION

The basic idea of origami is to plastically fold a plane into two, which are joined by a crease, along which the material is deconstructed [1–5]. Generally, thin films such as papers or plates, are used to create various origami art or structures via folding as they form creases easily. In principle, atomically thin 2D materials are ideal for origami manipulation as a crease in a 2D material can be created via linear atomic functionalization [4,6]. Such a technique is important for constructing various nanostructures of 2D materials and designing deformable and programmable devices [7–11].

Transition-metal dichalcogenides (TMDCs) are a well-explored family of 2D material similar to graphene insofar as they have desirable direct band gaps [12], high mobility values (up to a few hundred $cm^2\ V^{-1}\ s^{-1}$) [13], and intriguing chemical properties [14,15]. In comparison to graphene, a TMDC sheet has a very high bending stiffness (bending rigidity or flexural rigidity) [16–18], due to its three-atoms-thick sandwiched structure. Theoretically, the bending stiffness of a film is proportional to h^3, where h is the effective thickness of the materials, which is 0.3 nm and 0.077 nm for TMDC and graphene, respectively [19,20]. Thus, it can be estimated that the bending stiffness of a TMDC is about $\sim(0.3/0.077)^3$ or $\sim$60 times that of graphene. As such, highly curved TMDC nanostructures (e.g., nanotubes and fullerenes) are rarely observed. Indeed, most experimentally observed TMDC nanotubes [21–25] or fullerenelike cage structures [24–28] have diameters greater than $5 \sim 10$ nm, a sharp contrast to the diameter found in carbon nanotubes and fullerene, which can be around 0.4 to 0.7 nm [29,30]. This greatly limits the applications of TMDC and other few-layer-thick 2D materials.

To find an efficient route for reducing the energy penalty associated with bending TMDC nanostructures, we propose replacing bending the TMDC plane with the introduction of line defects, thus creating a sharp turn in the TMDC monolayer and facilitating TMDC origami. A line defect, such as the frequently observed sulfur vacancy lines [31–35] in a TMDC plane, can lead to an abrupt change of the plane direction with a constant energy penalty regardless of the width of the plane. Therefore, it can be applied to create stable and small TMDC nanostructures down to the nanometer scale. To fully elucidate the possibility of constructing TMDC nanostructures via origami or line defect engineering, we have systematically investigated the geometries and energetics of MoS_2 nanotubes and fullerenes via first-principles calculations. Our calculations show that nanotubes and fullerenes created via origami have superior thermal stability over bent nanostructures, especially for sizes at or below 5 nm. High-resolution transmission electron microscopy (HR-TEM) experiments were also carried out and provide evidence of sulfur line defects in highly curved TMDC nanoparticles. As a few examples, this approach can be used to produce many experimentally observed TMDC structures, such as the subnanometer TMDC nanowires, fullerenelike cages, clusters, and sharp turns in TMDC walls.

*dwh@phys.tsinghua.edu.cn
†f.ding@unist.ac.kr

II. METHODS

Computational details. Density functional theory (DFT) calculations were performed with the Vienna *ab initio* Simulation Package (VASP) [36]. The exchange-correlation functional was described by the Perdew-Burke-Ernzerhof version of generalized gradient approximation [37] and the core region by the projector augmented wave method [38] with the cutoff of plane wave set as 280 eV. A dense k-point mesh $1 \times 1 \times 11$ for the Brillouin zone sampling was used for one-dimensional periodic cells of MoS_2 nanotubes and nanoribbons that contained up to 300 atoms, and a $1 \times 1 \times 1$ mesh for MoS_2 fullerenes that contained up to 500 atoms. The vacuum layer was larger than 10 Å preventing interactions between neighboring images. Using the plane-wave-based total energy minimization, all structures were fully relaxed until the force on each atom was less than 0.01 eV/Å. The TEM-image simulations were carried out using the DR. PROBE software package [39]. *Ab initio* molecular dynamics (AIMD) simulations were also performed with VASP to check the thermal stability of fullerenes. All AIMD trajectories were run with the canonical ensemble (NVT) using a Nosé thermostat [40] at a temperature of 1100 K. The total time scales of the trajectories were from several to tens picoseconds (ps), with each simulation time step set as 1 femtosecond (fs).

Materials. First, graphene films were transferred onto TEM grids via a PMMA-assisted wet chemistry process. Monolayer and few-layer MoS_2 were then grown directly on graphene-supported TEM grids by chemical vapor deposition (CVD) as detailed in our previous work [41]. Multishelled fullerenelike structures were formed during the synthesis, and thus provided a platform for studying the bending properties.

Characterization. High-resolution transmission electron microscopy (HR-TEM) was conducted in a TEM (Titan G^2 80–300, FEI) with an aberration corrector on the imaging side and a monochrometer to reduce energy spread to ~0.15 eV. To reduce the radiation damage, this microscope was operated at an acceleration voltage of 80 kV and a dose rate of $\sim 1 \times 10^6$ e/nm^2 s for imaging. A negative spherical aberration (C3) of about -10 μm and a positive defocus were used. The images were filtered by an improved Wiener filtering method [42] to increase the signal-to-noise ratio for a better display. The contrast in HR-TEM images will change with defocus and thickness of the sample, which makes it difficult to obtain the exact atomic positions of Mo and S. Nevertheless, the missing S atom column in the bending region will change the atomic period of S atoms, and thus can be determined by image analysis.

III. RESULTS AND DISCUSSION

A. Line defect in TMDCs

Let us first consider the formation of a line defect in a MoS_2 plane. In the right inset of Fig. 1, a line defect is created by removing a chain of sulfur atoms along a zigzag direction from one side of the three-atom-thick material. After relaxation, the MoS_2 plane turns 38° towards the side missing the S atoms. Therefore, we can call such a line defect a crease in the 2D MoS_2 plane. The formation energy of a line defect

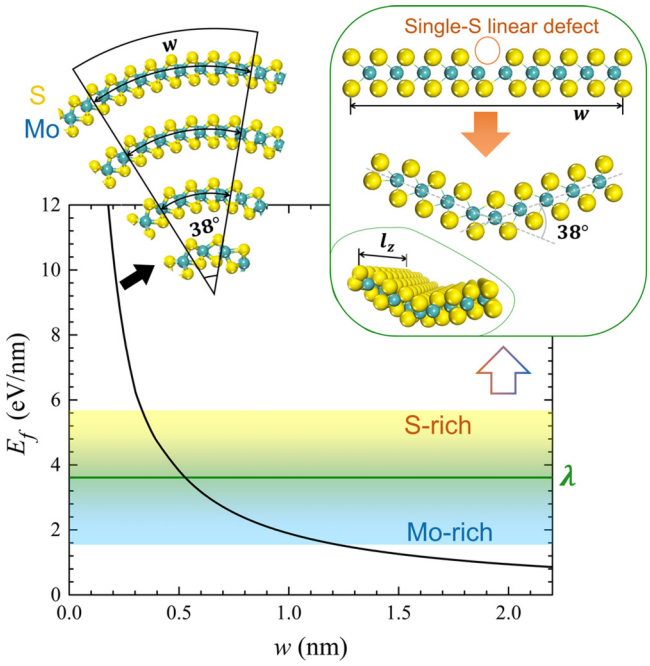

FIG. 1. Stability comparison between MoS_2 nanoribbons with and without line defect. The black curve is the formation energy of nanoribbons bent by 38°, as functions of ribbon width w. The left inset shows four nanoribbons of different widths that are all bent by 38°. The horizontal green line is the formation energy of a nanoribbon with a sulfur vacancy crease, λ, which is constant for different w. However, λ changes with different sulfur chemical potentials, μ_S, as denoted by the gradient blue-yellow shadow. The right inset is the front view of the initial and relaxed 2D and 3D atomic structures of MoS_2 nanoribbon with a sulfur vacancy crease.

per unit length is given by

$$\lambda = (E_{LD} - E_0 + \mu_S)/l_z, \tag{1}$$

where E_{LD} and E_0 are the calculated energies of the 2D MoS_2 plane with and without a line defect, respectively, and l_z is the length of the calculated MoS_2 plane. μ_S represents the chemical potential of a sulfur atom in the environment and its reasonable range is $[\frac{1}{2}(\varepsilon - \mu_{\text{Mo bulk}}), \mu_{S_8\text{ bulk}}]$, where the upper limit corresponds to a S-rich environment, the lower limit corresponds to a Mo-rich environment, and ε is the energy of MoS_2 monolayer [16]. The calculated λ ranges from 1.549 eV/nm for a Mo-rich environment to 5.677 eV/nm for a S-rich environment as shown in Fig. 1.

The energy penalty of a MoS_2 plane with a sulfur vacancy crease is independent of the width of the plane (w) because there is no elastic deformation distributed in the plane. In contrast, the formation energy of a bent MoS_2 plane is a function of width. The curvature energy of a MoS_2 plane with 38° bending angle as a function of its width (w) is shown as the black curve in Fig. 1. When w is less than a threshold width, the formation of a sulfur vacancy crease becomes more favorable than the bent MoS_2 plane. From Fig. 1, we can clearly see that the critical width ranges from 0.34–1.22 nm when μ_S varies from S-rich to Mo-rich environments. This analysis clearly shows that sulfur vacancy crease formation is more favorable in the width range of ~1 nm and therefore

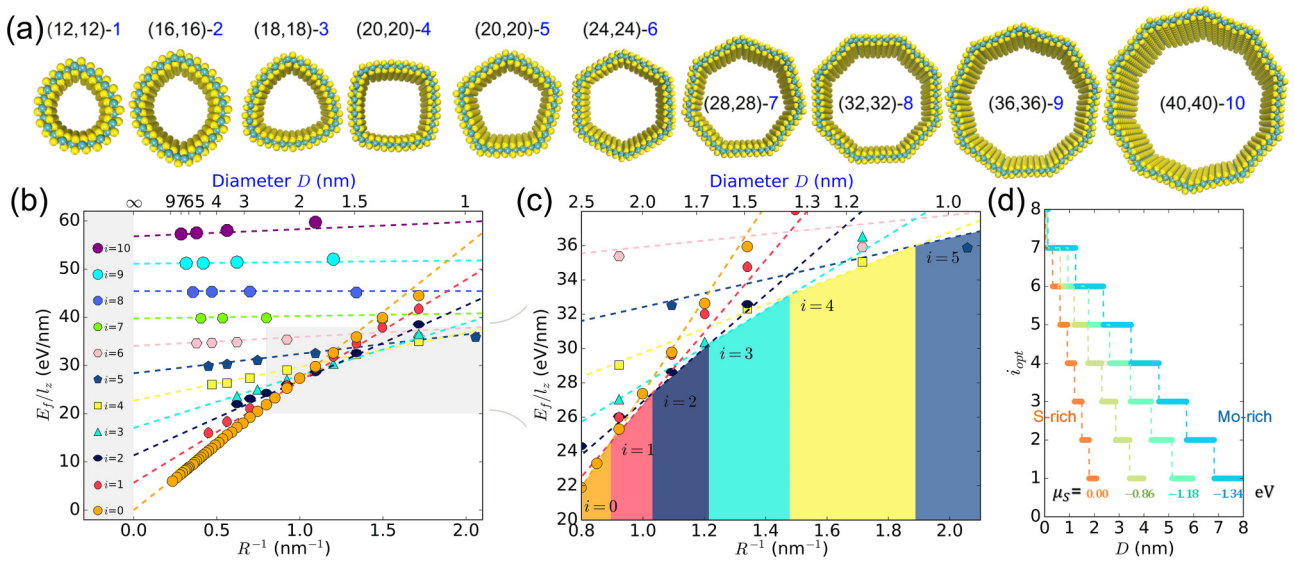

FIG. 2. Structures and stability of MoS_2 nanotubes with sulfur vacancy creases. (a) The relaxed structures of some MoS_2 nanotubes with different number of sulfur vacancy creases along the zigzag direction, (m, n)-i, where $i = 1, 2, \ldots, 10$. (b) The formation energy per unit length of MoS_2 nanotubes with i sulfur vacancy creases, as a function of the curvature of the original tube ($i = 0$) at $\mu_S = \mu_{S_8 bulk}$. Dashed lines are the linear fitting lines. (c) The enlarged view of the gray region shown in (b). (d) The optimal number of sulfur vacancy creases, i_{opt}, as a function of diameter of the nanotubes under different μ_S, where $\mu_S = \mu_{S_8 bulk}$ is set as zero.

it is the premium option for the creation of small TMDC nanostructures.

B. From TMDC nanotubes to subnanometer nanowire

Now let us consider the construction of small TMDC nanotubes by introducing a few sulfur vacancy creases along the tube axis direction. We start from a regular MoS_2 nanotube [43], denoted as (m, n). By introducing evenly distributed vacancy creases along the tube axis direction, the cross section of the tube will change from circular to polygonal shapes with convex, straight and concave edges gradually as the number of i varies from 0, 1, 2, etc., up to 10, in Fig. 2(a) and Fig. S1 in the Supplemental Material [44]. Here, we denote the nanotubes with i vacancy creases as (m, n)-i, with their formation energy $E_f^{(m,n)-i}$ defined as

$$E_f^{(m,n)-i} = E^{(m,n)-i} + i\mu_S - m\varepsilon, \tag{2}$$

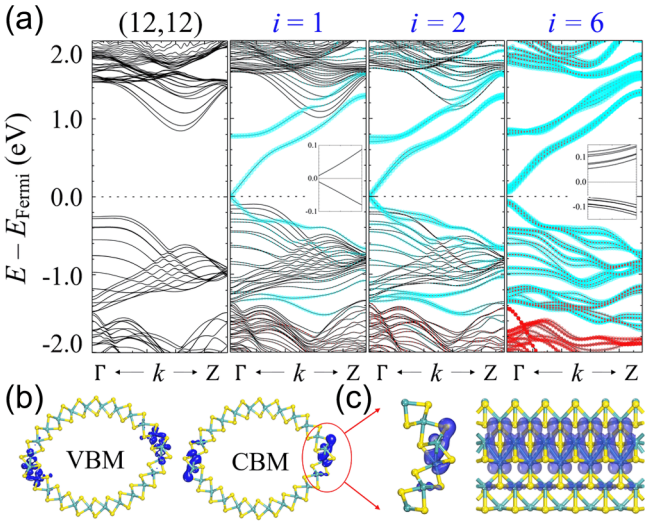

FIG. 3. Electronic properties of MoS_2 nanotubes with line defects. (a) Band structures of (12, 12) nanotube with different number of sulfur vacancy creases, $i = 0$, 1, 2, and 6. The blue and red dots are the contributions from Mo and S atoms around defects, respectively. The insets are enlarged views around the Fermi level. (b) Decomposed charge density of CBM and VBM at the Γ point for the (12,12)-2 tube. (c) Enlarged front and side views of (b).

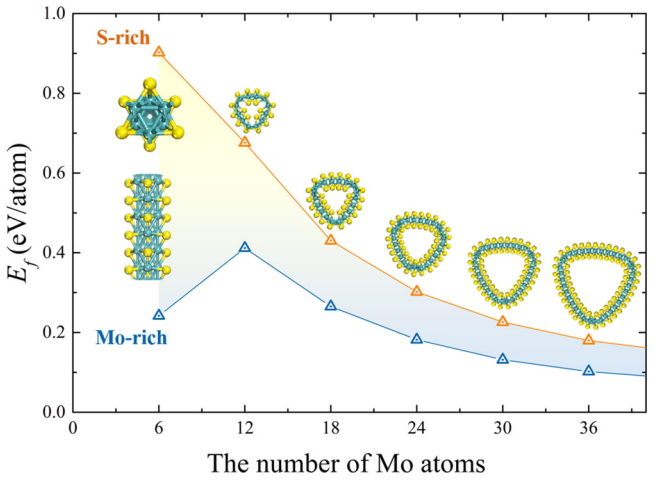

FIG. 4. Evolution from MoS_2 nanotube to nanowire. The formation energy per atom of zigzag MoS_2 nanotubes with three evenly distributed sulfur vacancy creases, in S-rich (orange dots) and Mo-rich (blue dots) environments. The insets are the corresponding optimal structures. The leftmost one is the smallest possible structure (top and front views), which is exactly the experimentally observed MoS_2 nanowire.

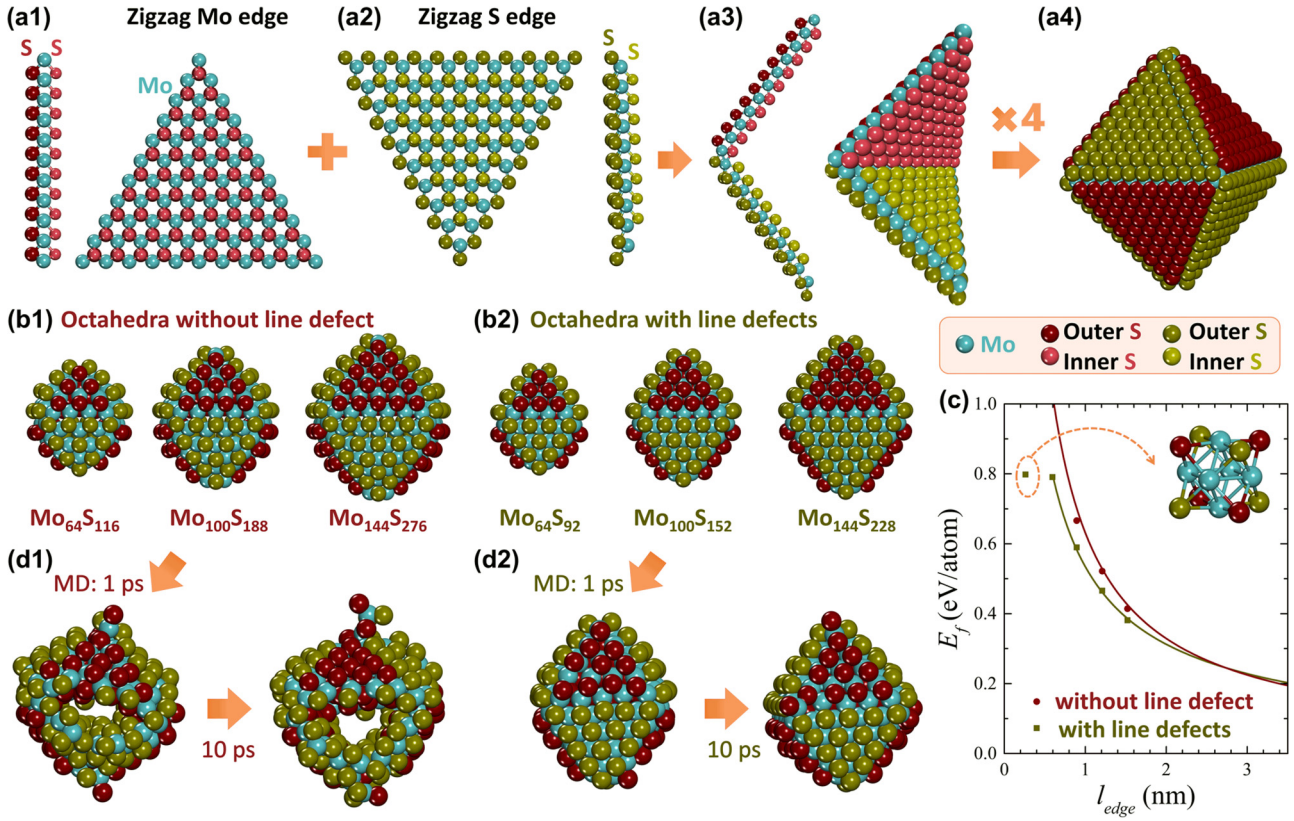

FIG. 5. Structures and stability of MoS_2 octahedron. (a) Construction of a MoS_2 octahedron nanocages with vacancy creases. Side view and top view of a regular MoS_2 triangle with ZZ Mo edges (a1) and ZZ S edges (a2). (a3) Side view and 3D views of a folded rhombus connected by (a1) and (a2). (a4) An integrated octahedron connected by four pieces of MoS_2 shown in (a3). (b) Top view of optimized structures without (b1) and with (b2) vacancy creases and the formation energy comparison for them (c). The inset in (c) is the Mo_6S_8 cluster, the smallest possible structure of octahedrons with vacancy creases, which has been well known as a catalyst for hydrodesulfurization. (d) Snapshots taken during the AIMD simulation of the MoS_2 octahedrons at 1100 K, without (d1) and with (d2) line defects.

where $E^{(m,n)-i}$ is the total energy of the nanotube, ε is the total energy per formula unit of a flat MoS_2 lattice, and i is the number of sulfur vacancy creases and also the number of missing S atoms in a unit cell. The data points in Figs. 2(b) and 2(c) show the calculated $E_f^{(m,n)-i}$ as a function of original tube curvature $R^{-1} = R^{-1}(m,n)$, assuming $\mu_S = \mu_{S_8 bulk}$ (S-rich). We can see from the figures that original nanotubes without line defects ($i = 0$) are global minima only for very small curvatures R^{-1} (large nanotubes). As R^{-1} gets larger (i.e., the nanotubes become smaller), the most favorable nanotubes become those incorporating sulfur vacancy creases.

As discussed above, introducing vacancy creases into nanotubes reduces the curvature energy penalty, with a penalty of the diameter-independent formation energy of the vacancy creases. Rolling a flat monolayer by 2π yields a circular nanotube. But, in case there are i vacancy creases in a MoS_2 layer, the required rolling angle is reduced to $2\pi - i\theta$. Thus $E_f^{(m,n)-i}$ can be estimated via

$$E_f^{(m,n)-i}/l_z = \frac{1}{2}B\left(\frac{2\pi - i\theta}{2\pi R}\right)^2 2\pi R + i\lambda, \qquad (3)$$

where B is the bending stiffness of MoS_2 monolayer (see Appendix).

As shown in Figs. 2(b) and 2(c), the linear relationship between $E_f^{(m,n)-i}/l_z$ and R^{-1} can be well fitted. The fitted formation energy of a sulfur vacancy crease of $\lambda = 5.67$ eV/nm is in very good agreement with the DFT result in a S-rich environment (i.e., $\mu_S = \mu_{S_8 bulk}$) shown in Fig. 1, while the fitted angle of $\theta = 44.4^\circ$ is also very close to that calculated with DFT, thus validating Eq. (3). All the structures involved are shown in Fig. S1. When the diameter of the nanotube is less than 2.2 nm the introduction of vacancy creases will greatly stabilize the nanotube. As the diameter gets smaller, more vacancy creases are required to further reduce the curvature energy. When $i = 7$, 8, and 9, the tube wall becomes very flat and therefore the curvature energy is nearly totally eliminated, however, the energy penalty of introducing too many vacancy creases is very large. When $i \geqslant 10$, the tube wall curves in a concave way, which further increases the curvature. Therefore structures where $i \geqslant 10$ cannot be the global minima for any types of nanotube. The results shown in Fig. 2(c) are based on a S-rich environment (i.e., $\mu_S = \mu_{S_8 bulk}$). It can be seen that the circular tube becomes the optimum structure when the diameter of the tube $D > 2.2$ nm (i.e., $R^{-1} < 0.45$ nm^{-1}). It is due to the fact that removing S atoms from TMDC, which is requires the creation of a line of vacancies, is not energetically favorable under the

S-rich environment. To have a full understanding of the effect of the environmental parameter, μ_S, on these systems, the optimum number of line defect, i_{opt}, as a function of D with different μ_S values was calculated [Fig. 2(d) and Eq. (A5) in the Appendix]. In a Mo-rich environment, the circular tubes become most favorable only if $D > 8.0$ nm and more vacancy creases are likely to be formed in the TMDC tubes. Under the real experimental condition of material synthesis, it is feasible to tune the concentration of sulfur or molybdenum to in turn, tune the concentration of line defects in the TMDC tubes.

In order to understand the electronic properties of the TMDC with vacancy creases, band structures were calculated [Fig. 3(a)]. Defect states near the Fermi energy are found for all structures and the band gap in all cases nearly vanishes due to the paired Mo-Mo bonds along the vacancy crease, which tend to be conducting. This is evident in the decomposed charge density of conductive band minimum (CBM) and valence band maximum (VBM) at the Γ point [Figs. 3(b) and 3(c)]. All band-gap data is in Table S1. As such, we can conclude that the conductivity of the TMDC nanotubes containing vacancy creases must be much higher than the bent circular nanotubes. This property is certainly very important for use as a building block in TMDC-based electronic devices. Note that the high conductivity of small MoS_2 nanotubes has been observed although the exact polygonal cross sections of the tubes were not seen directly [22].

Although the high stability of the polygonal TMDC nanotubes are clearly shown, there has been no direct experimental observation of these tubular structures until now. TMDC nanostructures have been well explored in many TMDC materials. Here we show that these TMDC nanowires can be considered as an extreme case of the polygonal nanotube, where the number of S atoms in the hollow of the tube becomes zero and many metal-metal bonds are built. In Fig. 4, zigzag MoS_2 nanotubes with three line defects are explored and it can be seen that nanotubes gradually evolve into the experimentally synthesized TMDC nanowire [45–48]. TMDC nanowires show a very high stability in a Mo-rich environment. This also shows that the nanotube structures have similar stabilities with nanowires and therefore their experimental synthesis is highly feasible, especially in a Mo-rich environment.

C. TMDC fullerenes

With the experience of constructing MoS_2 nanotubes and nanowires, we now turn to constructing small fullerene-like MoS_2 cages using this strategy of origami. Experimentally, nanooctahedrons are the most observed fullerene-like MoS_2 structures [26,27,49–51]. In such an octahedron, without introducing any sulfur vacancy creases, the eight facets are highly bent and simulated images of the modeled structures are far from the experimentally observed ones [26,27].

As shown in Fig. 5(a), we constructed MoS_2 octahedrons, regular ones without line defects [Fig. 5(b1)], and those applying the MoS_2 origami approach, which involves introducing 12 vacancy creases as the 12 edges of the octahedron structure [Fig. 5(b2)]. Comparing the octahedron structures with vacancy creases, the regular ones possess more rounded outlines. Figure 5(c) shows the formation energy of both structures as a function of their sizes, from which it can be clearly seen that introducing vacancy creases significantly decreases the formation energy of MoS_2 nanooctahedrons. It is interesting to note that the smallest nanooctahedrons with vacancy creases is the Mo_6S_8 cluster [the inset of Fig. 5(c)] which has been synthesized previously for use as catalysts (the Chevrel phases [52–56]). This again proves the validity and

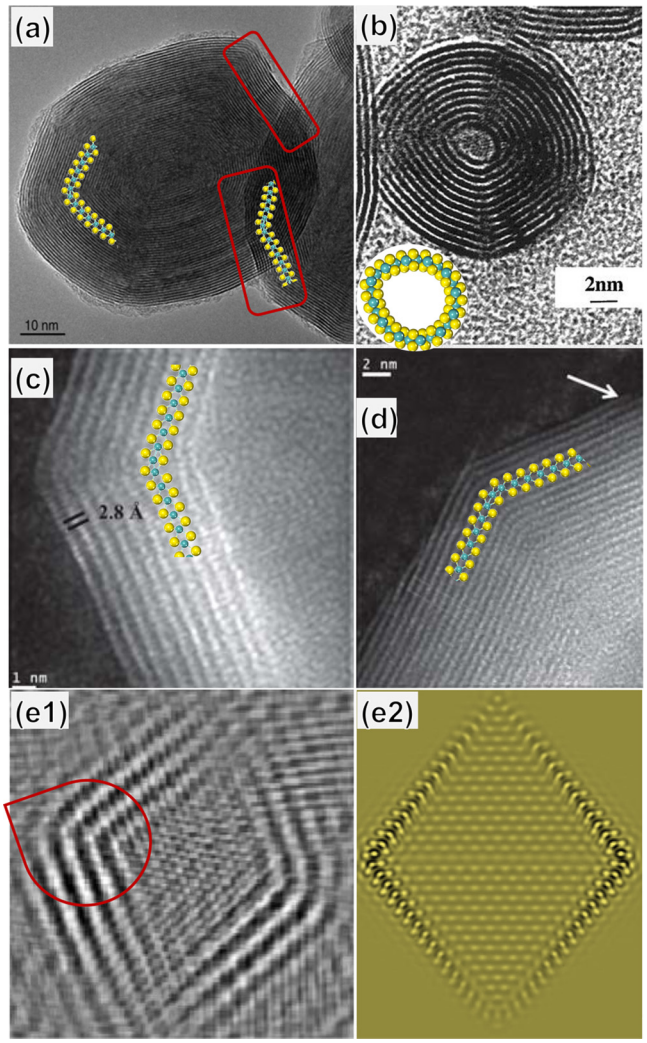

FIG. 6. Experimental evidences of vacancy creases in TMDC nanomaterials in the literature. (a) TEM micrograph of a MoS_2 nanoparticle, atomic models with creases are shown for comparison [57]. Copyright 2010, the Royal Society of Chemistry. The red rectangles denote two concavelike surfaces. (b) TEM image of a MoS_2 fullerene, in which the structures with vacancy creases are shown for comparison. Reproduced with permission [58]. Copyright 2000, American Chemical Society. (c) and (d) are scanning transmission electron microscopy images of MoS_2 nanotubes, in which the structures with vacancy creases are shown for comparison. Reproduced with permission [21]. Copyright 2010, the Royal Society of Chemistry. (e1) The fast Fourier transform filtered image of HR-TEM micrograph of a MoS_2 nanoparticle, reproduced with permission [27]. Copyright 2006, American Chemical Society. The red droplet denotes the sharp corners, which corresponds to creases of the MoS_2 plane. (e2) Simulated TEM image using octahedron with vacancy creases.

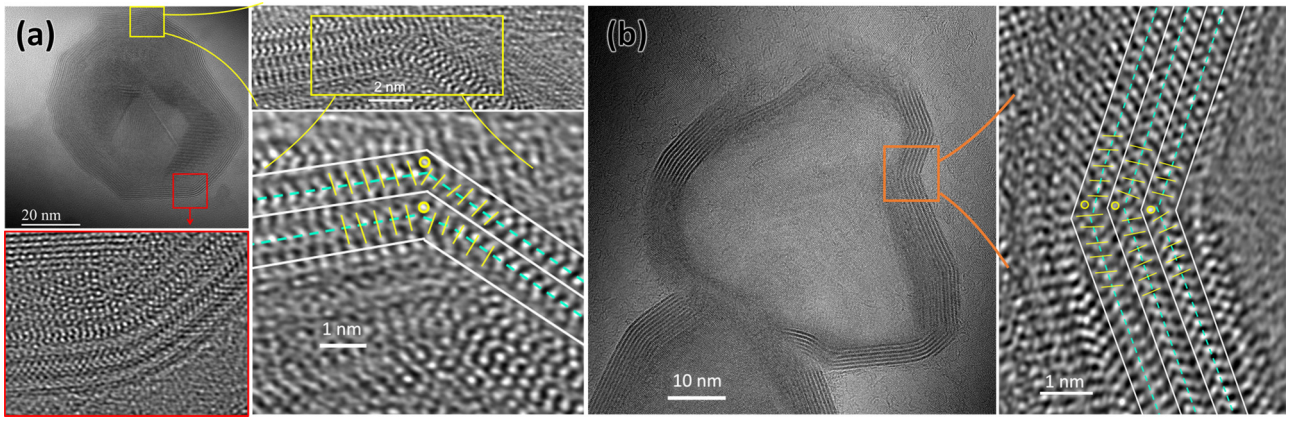

FIG. 7. Experimental evidences of sulfur vacancy creases. (a) HR-TEM image of the cross section of a MoS_2 nanoparticle contains both sharp (yellow) and blunt (red) turns. Enlarged views are also shown. To show the sulfur vacancy crease in the sharp turn, a structure model is overlaid on it, where the cyan dash lines are Mo planes, white lines are interlayer gaps, the yellow lines are pairs of S atoms, and the yellow circles in the corners are S atoms without corresponding inner S atoms (sulfur vacancy crease). (b) HR-TEM image of a MoS_2 nanoparticle with sharp turns. The region in the orange box has been enlarged and overlaid by a structural model.

feasibility of using the origami approach to predict various TMDC nanostructures.

Figure 5(d) shows snapshots of the AIMD simulations at a temperature of 1100 K. Without vacancy creases, the octahedron swelled up and collapsed after ∼1 ps, while the one with vacancy creases remains intact after 10 ps. Energy evolution during the AIMD simulations shows the high instability of the octahedron without vacancy creases (Fig. S2). These results show the superior stability of small-sized MoS_2 nanooctahedron with vacancy creases and strongly suggest the existence of such creases in TMDC fullerene like structures.

D. Experimental observations

Here we would like to address that the facet walls and sharp corners are broadly observed experimentally in TMDC nanostructures [21,22,25–28,50,51,57–62] and other 2D materials nanostructures such as GaSe onions and nanotubes [63], but these corners had no proper theoretical explanation until this work. For example, the bending structures of the MoS_2 walls are found to not be smooth but instead contain sharp turning angles [Figs. 6(a)–6(d)], and all these structures can be perfectly fitted by our simulated MoS_2 nanostructures with vacancy creases. Further, both the overall outline and the sharp corners in the HR-TEM images of the octahedral MoS_2 nanoparticle [27] can be perfectly fitted by the simulated TEM image of our octahedral model MoS_2 cage [Figs. 6(e1) and 6(e2)]. This shows that the experimentally synthesized TMDC cages are actually the nanostructure created via the proposed origami approach.

Although the general shapes of these nanostructures fit our theoretical model well, there is no direct characterization of the creases in previous studies. In order to confirm that these sharp turns are actually created via the formation of vacancy creases, we further carried out HR-TEM experiments to characterize the atomic arrangement in these highly bent surfaces. As shown in Fig. 7, both blunt and sharp corners are observed, and sulfur vacancy creases are found in the latter. Figure 7(a) shows the cross section of a MoS_2 nanoparticle, with blunt (red) and sharp (yellow) turns in the wall. The blunt turn has no sulfur vacancy crease and is smoothly bent with a quite large diameter (∼30 nm). The sharp turn, as shown in the enlarged view with structural model overlapped on it, has one more sulfur vacancy crease outside. Another case of MoS_2 nanoparticle with sharp turns is shown in Fig. 7(b), where the sulfur vacancy crease can be clearly seen in the cross-section image. Together with those presented in previous literatures, these observations prove that the sulfur vacancy crease is the dominating defect structure in these TMDC nanomaterials and is responsible for the shape changing and elastic energy relaxation.

IV. CONCLUSION

Through first-principles calculations and stability analysis, the feasibility of constructing very stable TMDC nanotubes and nanocages via the origami approach or introducing linear sulfur vacancy creases into the TMDC walls is confirmed. The experimentally observed TMDC nanowires and Chevrel phase cluster can be considered as the smallest structures obtained via this origami approach. Further, the crease structures of the TMDC or linear sulfur vacancy creases explain the experimentally observed sharp turns in TMDC walls and previously observed TMDC fullerenes are found to be the constructed TMDC octahedron. Our study opens a door to designing and synthesizing very small TMDC nanostructures for various applications. Finally, the proposed technique of 2D material origami can be easily applied to other few-atom-thick 2D materials.

ACKNOWLEDGMENTS

The authors acknowledge discussions with Dr. Chen Si, Dr. Xiaobin Chen, and Dr. Izaac Mitchell. The support from the Institute for Basic Science (IBS-R019-D1) of Korea is acknowledged. The computations were performed using the IBS-CMCM high-performance computing system *Cimulator*. W.D. acknowledges support from the Ministry of Science

and Technology of China (2016YFA0301001), and NSFC research grant (11674188). C.J. acknowledges support from NSFC research grant (51772265 and 61721005), the National Basic Research Program of China grant (2015CB921004).

APPENDIX: A CLASSICAL MODEL ON NANOTUBES WITH SULFUR VACANCY CREASES

We start from a regular MoS_2 nanotube as shown in Fig. 8(a). The perimeter l_0 and radius R of its cross section have a linear relationship with the number of Mo atoms in a circumference. We then create a certain number [$i = 5$ in Fig. 8(b)] of evenly distributed sulfur vacancy creases on the inside of the tube wall. Each sulfur vacancy crease carries a positive formation energy λ per unit length, and makes the tube rotate abruptly in the tangent direction, with an angle of θ. The tube wall then only needs to rotate a total angle of $2\pi - i\theta$ to form a closed circle. The cross section of the tube will present as an i-gon with less curved facets, whose perimeter l_0 is supposed to be unchanged. If we expand this less curved tube wall [Fig. 8(c)], we can see it has a smaller central angle, $2\pi - i\theta$, and a larger effective radius R_{eff}. Now the effective curvature k_{eff} of the wall of the i-gon tube can be calculated as

$$k_{\text{eff}} = \frac{1}{R_{\text{eff}}} = \frac{2\pi - i\theta}{l_0} = \frac{2\pi - i\theta}{2\pi R}. \tag{A1}$$

In this way, the overall curvature of tube wall will be greatly reduced and along with it, the curvature energy, at the cost of introducing a sulfur vacancy crease formation energy penalty. In this regard, its formation energy, $E_f^{(m,n)-i}$, can be viewed as being contributed by two parts, i.e., the curvature of tube wall and the presence of sulfur vacancy crease:

$$E_f^{(m,n)-i} = \tfrac{1}{2} B k_{\text{eff}}^2 l_0 l_z + i\lambda l_z, \tag{A2}$$

where l_z is the length of the tube in the periodic/axial direction, then $l_0 l_z$ is the surface area of the tube wall. B is the bending stiffness of the wall per area. Combine Eqs. (A1) and (A2) we can obtain the formation energy of a $(m, n) - i$ tube per unit length as

$$E_f^{(m,n)-i}/l_z = \frac{1}{2} B \frac{(2\pi - i\theta)^2}{2\pi R} + i\lambda. \tag{A3}$$

In our fitting of DFT results, the sum of squared residuals from the least-squares fitting method is 29.2, which involves 87 data points, with i in the range from 0–10, and within each i there are no less than four data points.

The optimal number of line defects for a certain tube size, i_{opt}, is calculated using Eq. (A3) as

$$\left.\frac{\partial E_f^{(m,n)-i}}{\partial i}\right|_{i=i_{\text{opt}}} = 0. \tag{A4}$$

Then we can get

$$i_{\text{opt}} = \frac{2\pi}{\theta} - \frac{\pi R \lambda}{B\theta^2}, \tag{A5}$$

where $E_f^{(m,n)-i}$ and λ are all dependent on μ_S.

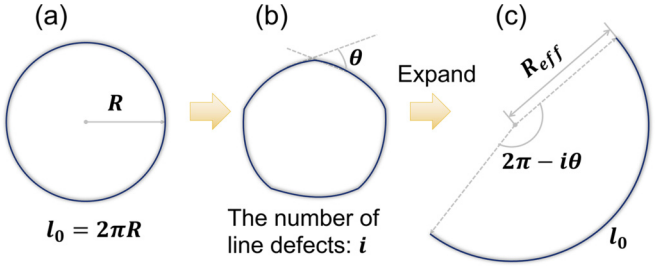

FIG. 8. A schematic view of introducing sulfur vacancy creases into a TMDC nanotube. (a) A regular nanotube. (b) A nanotube with surfur vacancy creases ($i = 5$). (c) Expand the nanotube wall.

[1] M. A. Dias, L. H. Dudte, L. Mahadevan, and C. D. Santangelo, Phys. Rev. Lett. **109**, 114301 (2012).
[2] L. H. Dudte, E. Vouga, T. Tachi, and L. Mahadevan, Nature Mater. **15**, 583 (2016).
[3] J. L. Silverberg, J.-H. Na, A. A. Evans, B. Liu, T. C. Hull, C. D. Santangelo, R. J. Lang, R. C. Hayward, and I. Cohen, Nature Mater. **14**, 389 (2015).
[4] S. Zhu and T. Li, ACS Nano **8**, 2864 (2014).
[5] Y. Aierken, O. Leenaerts, and F. M. Peeters, Phys. Rev. B **92**, 104104 (2015).
[6] T. W. Ebbesen and H. Hiura, Adv. Mater. **7**, 582 (1995).
[7] Z. Song *et al.*, Nature Commun. **5**, 3140 (2014).
[8] D. D. Han, Y. L. Zhang, J. N. Ma, Y. Q. Liu, B. Han, and H. B. Sun, Adv. Mater. **28**, 8328 (2016).
[9] J. Mu, C. Hou, H. Wang, Y. Li, Q. Zhang, and M. Zhu, Sci. Adv. **1**, e1500533 (2015).
[10] J. L. Silverberg, A. A. Evans, L. McLeod, R. C. Hayward, T. Hull, C. D. Santangelo, and I. Cohen, Science **345**, 647 (2014).
[11] S. Li, D. M. Vogt, D. Rus, and R. J. Wood, Proc. Natl. Acad. Sci. **114**, 13132 (2017).
[12] M. M. Ugeda *et al.*, Nature Mater. **13**, 1091 (2014).
[13] Q. H. Wang, K. Kalantar-Zadeh, A. Kis, J. N. Coleman, and M. S. Strano, Nature Nanotechnol. **7**, 699 (2012).
[14] W. Jamison and S. Cosgrove, ASLE Trans. **14**, 62 (1971).
[15] J. Wilson and A. Yoffe, Adv. in Phys. **18**, 193 (1969).
[16] W. Zhao, Y. Li, W. Duan, and F. Ding, Nanoscale **7**, 13586 (2015).
[17] K. Lai, W.-B. Zhang, F. Zhou, F. Zeng, and B.-Y. Tang, J. Phys. D: Appl. Phys. **49**, 185301 (2016).
[18] J. W. Jiang, Z. Qi, H. S. Park, and T. Rabczuk, Nanotechnology **24**, 435705 (2013).
[19] X. Wu, Z. Xu, and X. Zeng, Nano Lett. **7**, 2987 (2007).
[20] B. I. Yakobson, C. J. Brabec, and J. Bernholc, Phys. Rev. Lett. **76**, 2511 (1996).
[21] F. L. Deepak, A. Mayoral, A. J. Steveson, S. Mejía-Rosales, D. A. Blom, and M. José-Yacamán, Nanoscale **2**, 2286 (2010).

[22] M. Remskar, A. Mrzel, M. Virsek, M. Godec, M. Krause, A. Kolitsch, A. Singh, and A. Seabaugh, Nanoscale Res. Lett. **6**, 26 (2011).
[23] I. Kaplan-Ashiri, S. R. Cohen, K. Gartsman, V. Ivanovskaya, T. Heine, G. Seifert, I. Wiesel, H. D. Wagner, and R. Tenne, Proc. Natl. Acad. Sci. USA **103**, 523 (2006).
[24] L. Houben, A. Enyashin, Y. Feldman, R. Rosentsveig, D. Stroppa, and M. Bar-Sadan, J. Phys. Chem. C **116**, 24350 (2012).
[25] J. M. Gordon, E. A. Katz, D. Feuermann, A. Albu-Yaron, M. Levy, and R. Tenne, J. Mater. Chem. **18**, 458 (2008).
[26] A. N. Enyashin, M. Bar-Sadan, J. Sloan, L. Houben, and G. Seifert, Chem. Mater. **21**, 5627 (2009).
[27] M. Bar-Sadan, A. Enyashin, S. Gemming, R. Popovitz-Biro, S. Y. Hong, Y. Prior, R. Tenne, and G. Seifert, J. Phys. Chem. B **110**, 25399 (2006).
[28] A. Albu-Yaron *et al.*, Angew. Chem., Int. Ed. **50**, 1810 (2011).
[29] H. Y. Peng, N. Wang, Y. F. Zheng, Y. Lifshitz, J. Kulik, R. Q. Zhang, C. S. Lee, and S. T. Lee, Appl. Phys. Lett. **77**, 2831 (2000).
[30] N. Wang, Z.-K. Tang, G.-D. Li, and J. Chen, Nature (London) **408**, 50 (2000).
[31] A. N. Enyashin, M. Bar-Sadan, L. Houben, and G. Seifert, J. Phys. Chem. C **117**, 10842 (2013).
[32] M. Mahjouri-Samani *et al.*, Nano Lett. **16**, 5213 (2016).
[33] H. Liu, H. Zheng, F. Yang, L. Jiao, J. Chen, W. Ho, C. Gao, J. Jia, and M. Xie, ACS Nano **9**, 6619 (2015).
[34] S. Wang, G.-D. Lee, S. Lee, E. Yoon, and J. H. Warner, ACS Nano **10**, 5419 (2016).
[35] Z. Lin, B. R. Carvalho, E. Kahn, R. Lv, R. Rao, H. Terrones, M. A. Pimenta, and M. Terrones, 2D Mater. **3**, 022002 (2016).
[36] G. Kresse and J. Furthmüller, Comput. Mater. Sci **6**, 15 (1996).
[37] J. P. Perdew, K. Burke, and M. Ernzerhof, Phys. Rev. Lett. **77**, 3865 (1996).
[38] P. E. Blöchl, Phys. Rev. B **50**, 17953 (1994).
[39] http://www.er-c.org/barthel/drprobe/
[40] S. Nosé, J. Chem. Phys. **81**, 511 (1984).
[41] D. Zhu, H. Shu, F. Jiang, D. Lv, V. Asokan, O. Omar, J. Yuan, Z. Zhang, and C. Jin, npj 2D Materials Applications **1**, 8 (2017).
[42] F. Lin and C. Jin, Micron **50**, 1 (2013).
[43] G. Seifert, H. Terrones, M. Terrones, G. Jungnickel, and T. Frauenheim, Phys. Rev. Lett. **85**, 146 (2000).
[44] See Supplemental Material at http://link.aps.org/supplemental/10.1103/PhysRevMaterials.3.056001 for detailed classical model on nanotubes with line defects, optimal nanotube structures with line defects, energy profile of nanocages during molecular dynamics simulation, table of bandgap of MoS_2 nanotubes.
[45] J. Lin *et al.*, Nature Nanotechnol. **9**, 436 (2014).
[46] X. Sang, X. Li, W. Zhao, J. Dong, C. M. Rouleau, D. B. Geohegan, F. Ding, K. Xiao, and R. R. Unocic, Nature Commun. **9**, 2051 (2018).
[47] Y. Rong and J. H. Warner, ACS Nano **8**, 11907 (2014).
[48] A. L. Koh, S. Wang, C. Ataca, J. C. Grossman, R. Sinclair, and J. H. Warner, Nano Lett. **16**, 1210 (2016).
[49] P. Parilla, A. Dillon, K. Jones, G. Riker, D. Schulz, D. Ginley, and M. Heben, Nature (London) **397**, 114 (1999).
[50] A. N. Enyashin, S. Gemming, M. Bar-Sadan, R. Popovitz-Biro, S. Y. Hong, Y. Prior, R. Tenne, and G. Seifert, Angew. Chem. Int. Ed. Engl. **46**, 623 (2007).
[51] I. Alexandrou, N. Sano, A. Burrows, R. Meyer, H. Wang, A. Kirkland, C. Kiely, and G. Amaratunga, Nanotechnology **14**, 913 (2003).
[52] K. F. McCarty, J. Anderegg, and G. Schrader, J. Catal. **93**, 375 (1985).
[53] O. Peña, Physica C (Amsterdam) **514**, 95 (2015).
[54] R. K. Thompson, S. J. Hilsenbeck, T. J. Paskach, R. E. McCarley, and G. L. Schrader, J. Mol. Catal. A: Chem. **161**, 75 (2000).
[55] P. Murugan, V. Kumar, Y. Kawazoe, and N. Ota, Phys. Rev. A **71**, 063203 (2005).
[56] P. Murugan, V. Kumar, Y. Kawazoe, and N. Ota, J. Phys. Chem. A **111**, 2778 (2007).
[57] R. Tenne and M. Redlich, Chem. Soc. Rev. **39**, 1423 (2010).
[58] A. Zak, Y. Feldman, V. Alperovich, R. Rosentsveig, and R. Tenne, J. Am. Chem. Soc. **122**, 11108 (2000).
[59] A. Adini, M. Redlich, and R. Tenne, J. Mater. Chem. **21**, 15121 (2011).
[60] Y. Feldman, A. Zak, R. Popovitz-Biro, and R. Tenne, Solid State Sci. **2**, 663 (2000).
[61] S. Brown, J. Musfeldt, I. Mihut, J. Betts, A. Migliori, A. Zak, and R. Tenne, Nano Lett. **7**, 2365 (2007).
[62] N. Zink, H. A. Therese, J. Pansiot, A. Yella, F. Banhart, and W. Tremel, Chem. Mater. **20**, 65 (2007).
[63] U. K. Gautam, S. Vivekchand, A. Govindaraj, G. Kulkarni, N. Selvi, and C. Rao, J. Am. Chem. Soc. **127**, 3658 (2005).